Tensor decompositions in classical and quantum informatics

Piotr Gawron

AstroCeNT—Particle Astrophysics Science and Technology Centre
International Research Agenda
Nicolaus Copernicus Astronomical Center, Polish Academy of Sciences

Warsaw, October 7, 2022

Outline

AstroCeNT

Section 1

Motivation

Motivation

The motivation for this work was to study the applications of tensor decompositions in both:

- the theory of quantum multi-partite entanglement and
- classical signal processing.

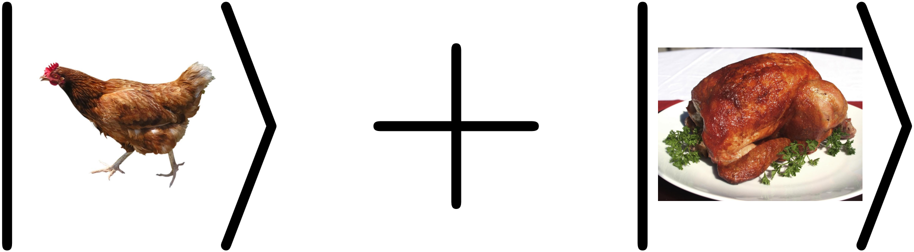

The talk is based on: Romaszewski, Michał, Piotr Gawron, and Sebastian Opozda. 2013. 'Dimensionality Reduction of Dynamic Mesh Animations Using HO-SVD'. Journal of Artificial Intelligence and Soft Computing Research 3 (4).

Section 2

Matrices

Matrix rank

- The *column rank* of a matrix **F** is the maximum number of linearly independent column vectors of **F**.
- The *row rank* of **F** is the maximum number of linearly independent row vectors of **F**.
- A result of fundamental importance in linear algebra is that the column rank and the row rank are always equal.

Singular Value Decomposition

Every matrix $\mathbf{F} \in \mathbb{C}^{I,J}$ can be written as the product

$$\mathbf{F} = \mathbf{U} \cdot \mathbf{S} \cdot \mathbf{V}^\dagger,$$

where

- $\mathbf{U} \in \mathbb{C}^{I,I}$, $\mathbf{V}^\dagger \in \mathbb{C}^{J,J}$ are unitary matrices,
- $\mathbf{S} \in \mathbb{R}^{I,J}$ matrix that is:
  - pseudo-diagonal: $\mathbf{S} = \mathrm{diag}(\sigma_1, \sigma_2, \dots, \sigma_{\min(I,J)})$,
  - its elements are ordered: $\sigma_1 \geq \sigma_2 \geq \dots \geq \sigma_{\min(I,J)} \geq 0$

The σ_i are *singular values* of $\mathbf{F}$, columns of $\mathbf{U}$ are *left singular vectors* and rows of $\mathbf{V}^\dagger$ are *right singular vectors*.

ASTROCENT

SVD figure

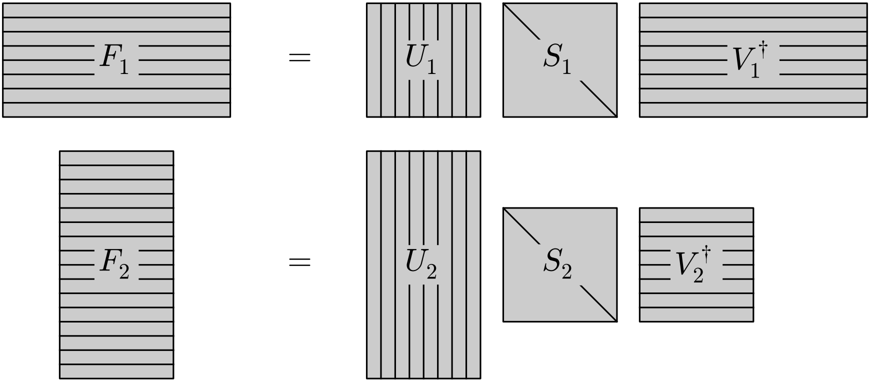

Figure: Visualisation of SVD.

AstroCeNT

SVD as rank revealing decompsition

Rank of a matrix $\mathbf{F}$ is equal to the number of its non-zero singular values $\sigma_i > 0$. Matrix $\mathbf{F}$ can be written in the form

$$\mathbf{F} = \sum_{i=1}^{\mathrm{rank}\,(\mathbf{F})} \sigma_i \mathbf{U}_{:,i} \circ \mathbf{V}^{\dagger}_{:,i},$$

where $\mathbf{A} = \mathbf{v} \circ \mathbf{w}$, $v \in \mathbb{C}^I, w \in \mathbb{C}^J, \mathbf{A} \in \mathbb{C}^{I,J}$, denotes outer product of vectors $\mathbf{v}$ and $\mathbf{w}$ *i.e.*:

$$(\mathbf{A})_{i,j} = (\mathbf{v} \circ \mathbf{w})_{i,j} = v_i w_j, \text{ for } 1 \leq i \leq I, 1 \leq j \leq J.$$

ASTROCENT

SVD and pure states bi-partite entanglement

Any bi-partite quantum pure state can be written as:

$$|\psi\rangle = \sum_{i=1,j=1}^{I,J} c_{i,j} |i\rangle |j\rangle \stackrel{SVD}{=} \sum_k \sigma_k |f_k\rangle |e_k\rangle ,$$

where $|f_k\rangle |e_k\rangle$ form orthonormal bases.

- The number of non-zero singular values σ_k of $(\mathbf{C})_{i,j} = c_{i,j}$ is often called the Schmidt number of state $|\psi\rangle$.
- Two pure bi-partite quantum states have the same entanglement structure if they have same singular values.
- Shanon entropy of σ_k is an entanglement measure of quantum states states i.e.:
$$E(|\psi\rangle) = \sum_k -\sigma_k \log_2(\sigma_k).$$

ASTROCENT

SVD-based approximation

By taking only first k singular values of $\mathbf{F}$ one can find rank-k approximation of matrix $\mathbf{F}$.

$$\mathbf{F} \approx \sum_{i=1}^{k} \sigma_i \mathbf{U}_{:,i} \circ \mathbf{V}^{\dagger}_{:,i}.$$

The larger k is the approximation is better.

ASTROCENT

Using SVD approximation for image compression

Figure: Original image: 1324×1725 pixels.

Using SVD approximation for image compression

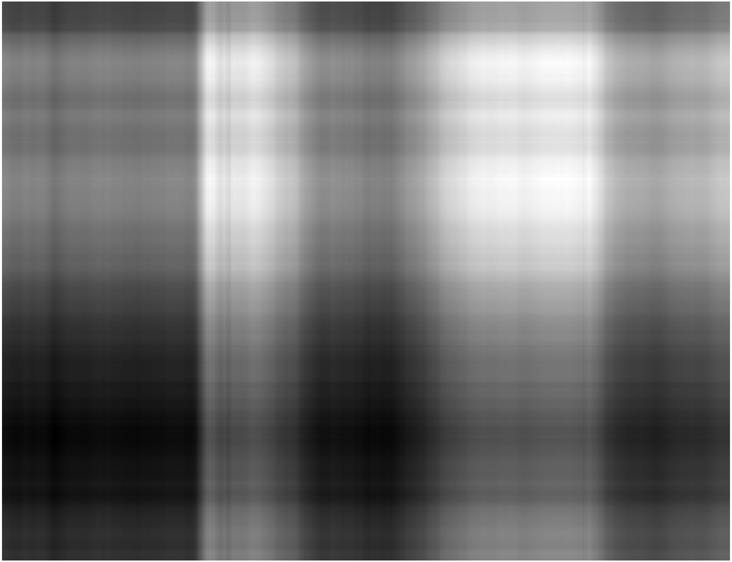

Figure: Rank 1 approximation.

Using SVD approximation for image compression

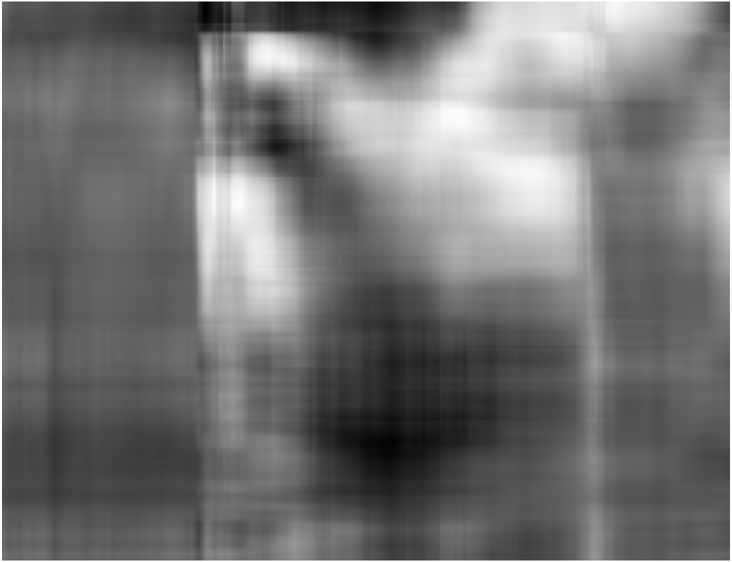

Figure: Rank 5 approximation.

Using SVD approximation for image compression

Figure: Rank 10 approximation.

Using SVD approximation for image compression

Figure: Rank 50 approximation.

Using SVD approximation for image compression

Figure: Rank 100 approximation.

Using SVD approximation for image compression

Figure: Rank 200 approximation.

SVD-based approximation of gestures

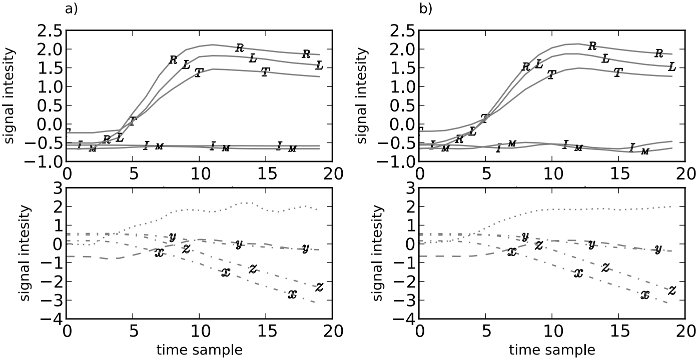

Fig. 1. A sample of the gestures dataset. The data are normalised and centred. Single realisation of *Cutting* gesture. Upper plot bending of fingers: *T*—thumb, *I*—index, *M*—middle, *R*—ring, *L*— little; lower plot: dashed line—palm roll, dotted line—palm pitch, *X Y Z*—palm position in space. (**a**) original data, (**b**) approximation reconstructed using only 20 first principal components.

Source: Gawron, Piotr, Przemysław Głomb, Jarosław Adam Miszczak, and Zbigniew Puchała. 2011. 'Eigengestures for Natural Human Computer Interface'. In Man-Machine Interactions 2, edited by Tadeusz Czachórski, Stanisław Kozielski, and Urszula Stańczyk, 103:49–56. Berlin, Heidelberg: Springer Berlin Heidelberg.

SVD-based approximation of gestures

Fig. 2 Relative Euclidean distance between the dataset and its approximation obtained using first *n* principal components.

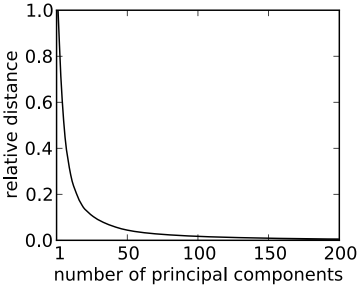

Source: Gawron, Piotr, Przemysław Głomb, Jarosław Adam Miszczak, and Zbigniew Puchała. 2011. 'Eigengestures for Natural Human Computer Interface'. In Man-Machine Interactions 2, edited by Tadeusz Czachórski, Stanisław Kozielski, and Urszula Stańczyk, 103:49–56. Berlin, Heidelberg: Springer Berlin Heidelberg.

SVD-based approximation of gestures

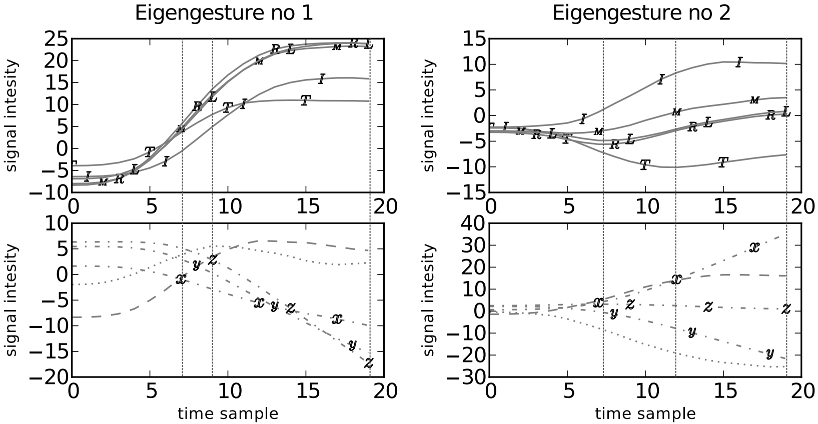

Source: Gawron, Piotr, Przemysław Głomb, Jarosław Adam Miszczak, and Zbigniew Puchała. 2011. 'Eigengestures for Natural Human Computer Interface'. In Man-Machine Interactions 2, edited by Tadeusz Czachórski, Stanisław Kozielski, and Urszula Stańczyk, 103:49–56. Berlin, Heidelberg: Springer Berlin Heidelberg.

SVD-based approximation of gestures

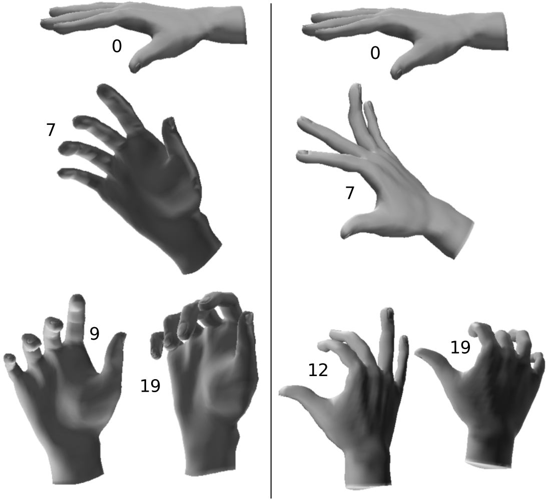

Fig. 3. Visualization of two first eigengestures (principal components). On top: normalized and centred plots of signals in time. Upper plot bending of fingers: T—thumb, I—index, M—middle, R—ring, L—little; lower plot: dashed line—palm roll, dotted line—palm pitch, $X\ Y\ Z$—palm position in space. At the bottom: shapes of hands in selected time moments. View is from the perspective of a person performing the gesture. For the sake of the clarity of the picture space position of the palm is omitted.

SVD-based approximation of 3D meshes

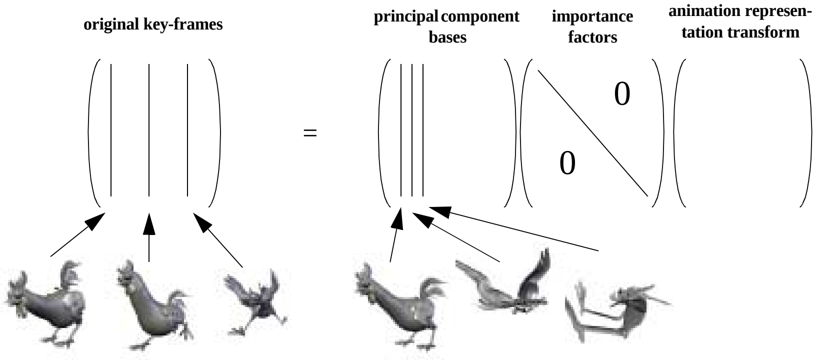

Figure 2: *The Principal Component Analysis for geometric animations illustrated.*

Source: Alexa, Marc, and Wolfgang Müller. 2000. 'Representing Animations by Principal Components'. Computer Graphics Forum 19 (3): 411–18.

Section 3

Tensors

Tensors

Let a tensor

$$\mathcal{T} = \{t_{i_1,i_2,\ldots,i_N}\}_{i_1,i_2,\ldots,i_N=1}^{I_1,I_2,\ldots,I_N} \in \mathbb{C}^{I_1,I_2,\ldots,I_N}$$

be given — we say that this tensor has N modes. Each of the indices corresponds to one of the modes *i.e.* i_l to mode l.

Tensors

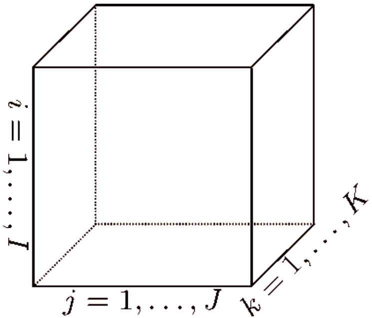

Figure: A 3-mode tensor.

ASTROCENT

Source: Kolda, T. G., and B. W. Bader. 2009. 'Tensor Decompositions and Applications'. SIAM Review 51 (3): 455–500.

Tensor — fibers

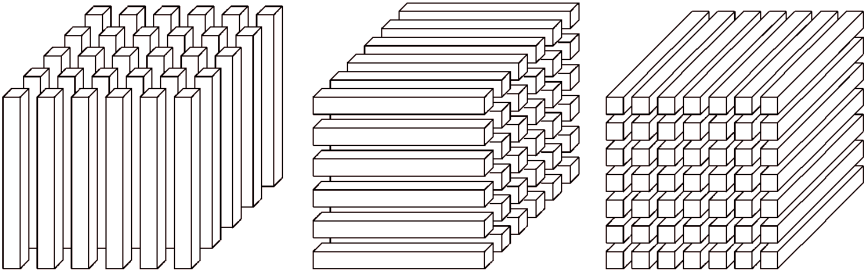

Figure: Fibers: Mode-1 (column) fibers) $\mathcal{T}_{:,j,k}$, Mode-2 (row) fibers $\mathcal{T}_{i,:,k}$, Mode-3 (tube) fibers $\mathcal{T}_{i,j,:}$.

ASTROCENT

Source: Kolda, T. G., and B. W. Bader. 2009. 'Tensor Decompositions and Applications'. SIAM Review 51 (3): 455–500.

Tensor — slices

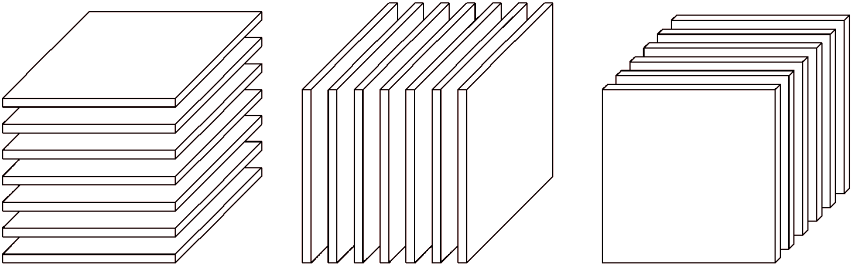

Figure: Slices: horizontal $\mathcal{T}_{i,:,:}$, lateral $\mathcal{T}_{:,j,:}$, frontal $\mathcal{T}_{:,:,k}$.

AstroCeNT

Source: Kolda, T. G., and B. W. Bader. 2009. 'Tensor Decompositions and Applications'. SIAM Review 51 (3): 455–500.

Tensor matrix multiplication

By *multiplication* of tensor $\mathcal{T}$ by matrix $\mathbf{U} = \{u_{i_l d}\}_{i_l,d=1}^{I_l,D} \in \mathbb{C}^{I_l,D}$ in mode l we define tensor $\mathcal{T}' \in \mathbb{C}^{I_1,\ldots,I_{l-1},D,I_{l+1},\ldots,I_N}$, such that:

$$\mathcal{T}' = (\mathcal{T} \times_l \mathbf{U})_{i_1\ldots i_{l-1} d\, i_{l+1}\ldots i_N} = \sum_{i_l=1}^{I_l} t_{i_1 i_2 \ldots i_l \ldots i_N} u_{i_l d}.$$

ASTROCENT

Tensors unfolding

By *unfolding* tensor $\mathcal{T}$ in mode l we define matrix $\mathbf{T}_{(l)}$ such that

$$(\mathbf{T}_{(l)})_{i,j} = t_{i_1 \dots i_{l-1} j \, i_{l+1} \dots i_N},$$

where

$$i = 1 + \sum_{\substack{k=1 \\ l \neq l}}^{N} J_k \quad \text{and} \quad J_k = \prod_{\substack{m=1 \\ m \neq l}}^{k-1} I_m.$$

AstroCeNT

Tensors unfolding — exmaple

$$\mathcal{A}_{1,:,:} = \begin{pmatrix} 0 & 1 & 2 & 3 \\ 4 & 5 & 6 & 7 \\ 8 & 9 & 10 & 11 \end{pmatrix} \mathcal{A}_{2,:,:} = \begin{pmatrix} 12 & 13 & 14 & 15 \\ 16 & 17 & 18 & 19 \\ 20 & 21 & 22 & 23 \end{pmatrix}$$

$$\mathbf{A}_{(1)} = \begin{pmatrix} 0 & 4 & 8 & 1 & 5 & 9 & 2 & 6 & 10 & 3 & 7 & 11 \\ 12 & 16 & 20 & 13 & 17 & 21 & 14 & 18 & 22 & 15 & 19 & 23 \end{pmatrix}$$

$$\mathbf{A}_{(2)} = \begin{pmatrix} 0 & 12 & 1 & 13 & 2 & 14 & 3 & 15 \\ 4 & 16 & 5 & 17 & 6 & 18 & 7 & 19 \\ 8 & 20 & 9 & 21 & 10 & 22 & 11 & 23 \end{pmatrix}$$

$$\mathbf{A}_{(3)} = \begin{pmatrix} 0 & 12 & 4 & 16 & 8 & 20 \\ 1 & 13 & 5 & 17 & 9 & 21 \\ 2 & 14 & 6 & 18 & 10 & 22 \\ 3 & 15 & 7 & 19 & 11 & 23 \end{pmatrix}$$

ASTROCENT

Sub-tensors

Given tensor $\mathcal{T}$, a new *sub-tensor* $\mathcal{T}_{i_n=\alpha}$ can be created:

$$\mathcal{T}_{i_l=\alpha} = \{t_{i_1 i_2 \ldots i_{l-1} i_{l+1} \ldots i_n}\}_{i_1=1, i_2=1, \ldots, i_l=\alpha, \ldots, i_n=1}^{I_1, I_2, \ldots, \alpha, \ldots, I_N} \in \mathbb{C}^{I_1, I_2, \ldots, 1, \ldots, I_N}.$$

ASTROCENT

Tensor rank

- The *n-rank of tensor* $\mathcal{A}$, denoted by $R_n = \mathrm{rank}_n(\mathcal{A})$ is the rank of the matrix $\mathbf{A}_{(n)}$.
- An N-mode tensor $\mathcal{A} \in \mathbb{C}^{I_1, I_2, \ldots, I_N}$ has rank 1 when it equals to the outer product of N vectors $\mathbf{v}^{(1)} \in \mathbb{C}^{I_1}, \mathbf{v}^{(2)} \in \mathbb{C}^{I_2}, \ldots, \mathbf{v}^{(N)} \in \mathbb{C}^{I_N}$, i.e.

$$\mathcal{A} = \mathbf{v}^{(1)} \circ \mathbf{v}^{(2)} \circ \ldots \circ \mathbf{v}^{(N)},$$

where $\circ$ is outer product of vectors.

$$(\mathcal{A})_{i_1, i_2, \ldots, i_N} = (\mathbf{v}^{(1)} \circ \mathbf{v}^{(2)} \circ \ldots \circ \mathbf{v}^{(N)})_{i_1, i_2, \ldots, i_N} = v_{i_1}^{(1)} v_{i_2}^{(2)} \ldots v_{i_N}^{(N)},$$

for $1 \leq i_n \leq I_N, 1 \leq n \leq N$.

ASTROCENT

Rank one tensor

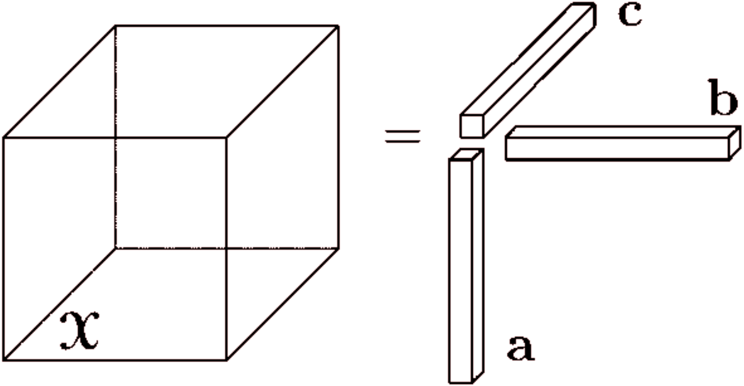

Figure: Rank one tensor $\mathcal{X} = \mathbf{a} \circ \mathbf{b} \circ \mathbf{c}$

Tensor rank, cnt.

- The *rank of N-mode tensor* $\mathcal{A}$, denoted by $R = \mathrm{rank}(A)$, is the minimal number of rank 1 tensors that yield $\mathcal{A}$ in a linear combination.

AstroCeNT

Rank one tensor

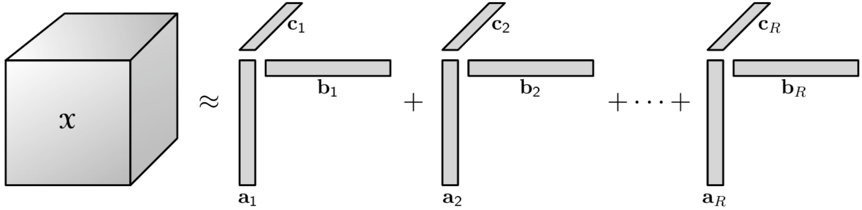

Figure: Sum of rank one tensors.

Tensor rank, cnt.

- The main difference between matrices and higher-order tensors is the fact that the rank is not necessarily equal to an n-rank, even when all the n-ranks are the same.
- From the definitions it is clear that always $R_n \leq R$.

ASTROCENT

Tensor rank — example 1

The tensor

$$\mathcal{A}_{1,:,:} = \begin{pmatrix} 1 & 1 \\ 0 & 0 \end{pmatrix} \mathcal{A}_{2,:,:} = \begin{pmatrix} 1 & 0 \\ 0 & 0 \end{pmatrix},$$

having the following unfoldings:

$$\mathbf{A}_{(1)} = \begin{pmatrix} 1 & 0 & 1 & 0 \\ 1 & 0 & 0 & 0 \end{pmatrix} \mathbf{A}_{(2)} = \begin{pmatrix} 1 & 1 & 1 & 0 \\ 0 & 0 & 0 & 0 \end{pmatrix} \mathbf{A}_{(3)} = \begin{pmatrix} 1 & 1 & 0 & 0 \\ 1 & 0 & 0 & 0 \end{pmatrix}$$

has $R_1 = 2, R_2 = 1, R_3 = 2$.

Tensor rank — example 2

- The tensor

$$\mathcal{A}_{1,:,:} = \begin{pmatrix} 0 & 1 \\ 1 & 0 \end{pmatrix} \mathcal{A}_{2,:,:} = \begin{pmatrix} 1 & 0 \\ 0 & 0 \end{pmatrix}$$

  has all n-ranks equal $R_1 = R_2 = R_3 = 2$.
- But $\text{rank}(\mathcal{A}) = 3$:

$$\mathcal{A} = \mathbf{x}_2 \circ \mathbf{y}_1 \circ \mathbf{z}_1 + \mathbf{x}_1 \circ \mathbf{y}_2 \circ \mathbf{z}_1 + \mathbf{x}_1 \circ \mathbf{y}_1 \circ \mathbf{z}_2,$$

$$\mathbf{x}_1 = \mathbf{y}_1 = \mathbf{z}_1 = \begin{pmatrix} 1 \\ 0 \end{pmatrix} \quad \mathbf{x}_2 = \mathbf{y}_2 = \mathbf{z}_2 = \begin{pmatrix} 0 \\ 1 \end{pmatrix}.$$

AstroCeNT

Breaking NEWS! AlphaTensor

Source: Cover image — Adam Cain/Domhnall Malone/DeepMind

AlphaTensor

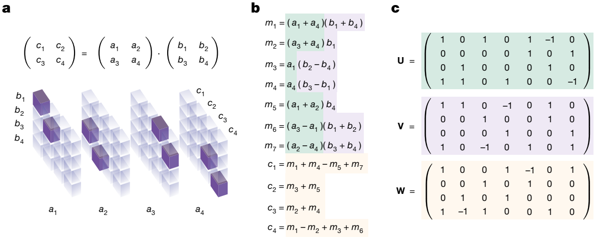

Fig. 1 | Matrix multiplication tensor and algorithms. a, Tensor $\mathcal{T}_2$ representing the multiplication of two 2 × 2 matrices. Tensor entries equal to 1 are depicted in purple, and 0 entries are semi-transparent. The tensor specifies which entries from the input matrices to read, and where to write the result. For example, as $c_1 = a_1b_1 + a_2b_3$, tensor entries located at (a_1, b_1, c_1) and (a_2, b_3, c_1) are set to 1. **b**, Strassen's algorithm[2] for multiplying 2 × 2 matrices using 7 multiplications. **c**, Strassen's algorithm in tensor factor representation. The stacked factors **U**, **V** and **W** (green, purple and yellow, respectively) provide a rank-7 decomposition of $\mathcal{T}_2$ (equation (1)). The correspondence between arithmetic operations (**b**) and factors (**c**) is shown by using the aforementioned colours.

Source: Fawzi, Alhussein, Matej Balog, Aja Huang, Thomas Hubert, Bernardino Romera-Paredes, Mohammadamin Barekatain, Alexander Novikov, et al. 2022. ‘Discovering Faster Matrix Multiplication Algorithms with Reinforcement Learning’. Nature 610 (7930): 47–53.

AlphaTensor

Algorithm 1

A meta-algorithm parameterized by $\{\mathbf{u}^{(r)}, \mathbf{v}^{(r)}, \mathbf{w}^{(r)}\}_{r=1}^{R}$ for computing the matrix product $\mathbf{C}=\mathbf{AB}$. It is noted that R controls the number of multiplications between input matrix entries.

Parameters: $\{\mathbf{u}^{(r)}, \mathbf{v}^{(r)}, \mathbf{w}^{(r)}\}_{r=1}^{R}$: length-$n^2$ vectors such that $\mathcal{T}_n = \sum_{r=1}^{R} \mathbf{u}^{(r)} \otimes \mathbf{v}^{(r)} \otimes \mathbf{w}^{(r)}$

Input: $\mathbf{A}, \mathbf{B}$: matrices of size $n \times n$

Output: $\mathbf{C}=\mathbf{AB}$

(1) **for** $r=1, \ldots, R$ **do**

(2) $\quad m_r \leftarrow (u_1^{(r)} a_1 + \cdots + u_{n^2}^{(r)} a_{n^2})(v_1^{(r)} b_1 + \cdots + v_{n^2}^{(r)} b_{n^2})$

(3) **for** $i=1, \ldots, n^2$ **do**

(4) $\quad c_i \leftarrow w_i^{(1)} m_1 + \cdots + w_i^{(R)} m_R$

return $\mathbf{C}$

Source: Fawzi, Alhussein, Matej Balog, Aja Huang, Thomas Hubert, Bernardino Romera-Paredes, Mohammadamin Barekatain, Alexander Novikov, et al. 2022. 'Discovering Faster Matrix Multiplication Algorithms with Reinforcement Learning'. Nature 610 (7930): 47–53.

AlphaTensor

Size (n, m, p)	Best method known	Best rank known	AlphaTensor rank Modular	Standard
(2, 2, 2)	(Strassen, 1969)[2]	7	7	7
(3, 3, 3)	(Laderman, 1976)[15]	23	23	23
(4, 4, 4)	(Strassen, 1969)[2] $(2,2,2) \otimes (2,2,2)$	49	47	49
(5, 5, 5)	(3, 5, 5) + (2, 5, 5)	98	96	98
(2, 2, 3)	(2, 2, 2) + (2, 2, 1)	11	11	11
(2, 2, 4)	(2, 2, 2) + (2, 2, 2)	14	14	14
(2, 2, 5)	(2, 2, 2) + (2, 2, 3)	18	18	18
(2, 3, 3)	(Hopcroft and Kerr, 1971)[16]	15	15	15
(2, 3, 4)	(Hopcroft and Kerr, 1971)[16]	20	20	20
(2, 3, 5)	(Hopcroft and Kerr, 1971)[16]	25	25	25
(2, 4, 4)	(Hopcroft and Kerr, 1971)[16]	26	26	26
(2, 4, 5)	(Hopcroft and Kerr, 1971)[16]	33	33	33
(2, 5, 5)	(Hopcroft and Kerr, 1971)[16]	40	40	40
(3, 3, 4)	(Smirnov, 2013)[18]	29	29	29
(3, 3, 5)	(Smirnov, 2013)[18]	36	36	36
(3, 4, 4)	(Smirnov, 2013)[18]	38	38	38
(3, 4, 5)	(Smirnov, 2013)[18]	48	47	47
(3, 5, 5)	(Sedoglavic and Smirnov, 2021)[19]	58	58	58
(4, 4, 5)	(4, 4, 2) + (4, 4, 3)	64	63	63
(4, 5, 5)	$(2,5,5) \otimes (2,1,1)$	80	76	76

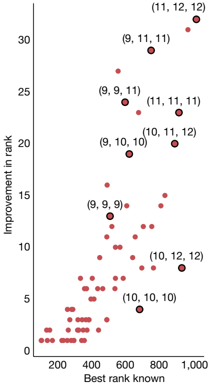

Fig. 3 | Comparison between the complexity of previously known matrix multiplication algorithms and the ones discovered by AlphaTensor. Left: column (n, m, p) refers to the problem of multiplying $n \times m$ with $m \times p$ matrices. The complexity is measured by the number of scalar multiplications (or equivalently, the number of terms in the decomposition of the tensor). 'Best rank known' refers to the best known upper bound on the tensor rank (before this paper), whereas 'AlphaTensor rank' reports the rank upper bounds obtained with our method, in modular arithmetic ($\mathbb{Z}_2$) and standard arithmetic. In all cases, AlphaTensor discovers algorithms that match or improve over known state of the art (improvements are shown in red). See Extended Data Figs. 1 and 2 for examples of algorithms found with AlphaTensor. Right: results (for arithmetic in $\mathbb{R}$) of applying AlphaTensor-discovered algorithms on larger tensors. Each red dot represents a tensor size, with a subset of them labelled. See Extended Data Table 1 for the results in table form. State-of-the-art results are obtained from the list in ref. [64].

Source: Fawzi, Alhussein, Matej Balog, Aja Huang, Thomas Hubert, Bernardino Romera-Paredes, Mohammadamin Barekatain, Alexander Novikov, et al. 2022. 'Discovering Faster Matrix Multiplication Algorithms with Reinforcement Learning'. Nature 610 (7930): 47–53.

Tensor scalar product

The *scalar product* $\langle \mathcal{A}, \mathcal{B} \rangle$ of tensors $\mathcal{A}, \mathcal{B} \in \mathbb{C}^{I_1, I_2, \ldots, I_N}$ is defined as

$$\langle \mathcal{A}, \mathcal{B} \rangle = \sum_{i_1=1}^{I_1} \sum_{i_2=1}^{I_2} \ldots \sum_{i_N=1}^{I_N} b^*_{i_1, i_2, \ldots, i_n} a_{i_1, i_2, \ldots, i_n}.$$

We say that if scalar product of tensors equals 0, then they are orthogonal. The *Frobenius norm* of tensor $\mathcal{T}$ is given by

$$||\mathcal{T}|| = \sqrt{\langle \mathcal{T}, \mathcal{T} \rangle}.$$

Higher Order Singular Value Decomposition (HO-SVD)

Given tensor $\mathcal{T}$, in order to find its HO-SVD, in the form of the so called Tucker operator $[\![\mathcal{C}; \mathbf{U}^{(1)}, \ldots, \mathbf{U}^{(N)}]\!]$, such that $\mathcal{C} \in \mathbb{C}^{I_1,\ldots,I_N}$ and $\mathbf{U}^{(k)} \in \mathbb{C}^{I_k \times I_k}$ are unitary matrices following algorithm can be used.

ASTROCENT

HO-SVD algorithm

Input: Tensor $\mathcal{T}$
Output: Tucker operator $[\![\mathcal{C}; \mathbf{U}^{(1)}, \dots, \mathbf{U}^{(N)}]\!]$
for $n \in \{1, \dots, N\}$ **do**
    $\mathbf{U}^{(n)} =$ left singular vectors of $\mathbf{T}_{(n)}$ in unfolding n;
end
$\mathcal{C} = \mathcal{T} \times_1 \mathbf{U}^{(1)\dagger} \times_2 \mathbf{U}^{(2)\dagger} \dots \times_N \mathbf{U}^{(N)\dagger}$;
return $[\![\mathcal{C}; \mathbf{U}^{(1)}, \dots, \mathbf{U}^{(N)}]\!]$;

Algorithm 1: HO-SVD algorithm

ASTROCENT

Tensor $\mathcal{C}$ is called the core tensor and has the following useful properties.

- Reconstruction:

$$\mathcal{T} = \mathcal{C} \times_1 \mathbf{U}^{(1)} \times_2 \mathbf{U}^{(2)} \times_3 \ldots \times_N \mathbf{U}^{(N)},$$

  where $\mathbf{U}^{(i)}$ are unitary matrices;

- Orthogonality:

$$\langle \mathcal{C}_{i_l=\alpha}, \mathcal{C}_{i_l=\beta} \rangle = 0$$

  for all possible values of l, α and β, such that $\alpha \neq \beta$;

- Order of sub-tensor norms:

$$||\mathcal{C}_{i_n=1}|| \geq ||\mathcal{C}_{i_n=2}|| \geq \ldots \geq ||\mathcal{C}_{i_n=I_n}|| \geq 0$$

  for all n.

ASTROCENT

Quantum multi-partite entanglement

- Assuming that all $\sigma_i^{(n)}$ singular values of unfoldings $\mathbf{T}_{(n)}$ are all distinct, then

$$\mathcal{C}' = \mathcal{C} \times_1 \Theta^{(1)} \times_2 \Theta^{(2)} \times_3 \ldots \times_N \Theta^{(N)},$$

  where $\Theta^{(n)} = \mathrm{diag}(e^{\imath\theta_1^{(n)}}, e^{\imath\theta_2^{(n)}}, \ldots e^{\imath\theta_{I_n}^{(n)}})$, then $\mathcal{C}'$ is also core tensor of $\mathcal{T}$. Therefore HO-SVD decomposition is not unique.
- The case where singular values are not distinct is more complicated and will be omitted here.

ASTROCENT

Quantum multi-partite entanglement cnt.

Any multi-partite quantum state $|\psi\rangle \in \mathbb{C}^{I_1,I_2,\ldots,I_N}$ can be expressed as:

$$|\psi\rangle = \sum_{i_1=1,i_1=2,\ldots,i_N=1}^{I_1,I_2,\ldots,I_N} t_{i_1,i_2,\ldots,i_N} |i_1\rangle |i_2\rangle \ldots |i_N\rangle .$$

- The core tensor associated with group $\bigotimes_{n=1}^{N} \Theta^{(n)}$ is the canonical form of the multipartite pure state and is the entanglement class under local unitary equivalence.
- Given two quantum states, using HOSVD, it is possible to determine if they are LU equivalent. Details can be found in: Jun-Li Li and Cong-Feng Qiao. Classification of arbitrary multipartite entangled states under local unitary equivalence. *Journal of Physics A: Mathematical and Theoretical*, 46(7):075301, 2013.

AstroCeNT

Approxmiation

Larger values of a core tensor are denoted by low values of indices. This property is the basis for the development of compression algorithms based on HO-SVD.

Formally

$$\tilde{\mathcal{T}} = \tilde{\mathcal{C}} \times_1 \tilde{\mathbf{U}}^{(1)} \times_2 \tilde{\mathbf{U}}^{(2)} \times_3 \ldots \times_N \tilde{\mathbf{U}}^{(N)},$$

where

$$\tilde{\mathcal{C}} = \{c_{i_1,i_2,\ldots,i_n}\}_{i_1,i_2,\ldots,i_n=1}^{R_1,R_2,\ldots,R_N} \in \mathbb{C}^{R_1,R_2,\ldots,R_N}$$

is a truncated tensor in such a way that in each mode l indices span from 1 to $R_l \leq I_l$ and $\tilde{\mathbf{U}}^{(l)} \in \mathbb{C}^{R_l \times I_l}$ matrices whose columns are orthonormal and rows form orthonormal basis in respective vector spaces.

ASTROCENT

Approxmiation

A visualization of 3-mode truncated tensor.

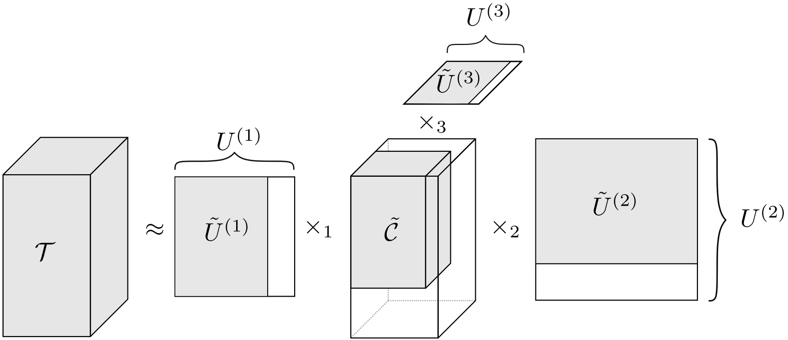

Figure: Truncated HO-SVD decomposition of tensor $\mathcal{T}$. Its approximation, tensor $\tilde{\mathcal{T}}$, can be reconstructed from a truncated tucker operator $[\![\tilde{\mathcal{C}}; \tilde{\mathbf{U}}^{(1)}, \tilde{\mathbf{U}}^{(2)}, \tilde{\mathbf{U}}^{(3)}]\!]$.

AstroCeNT

Approxmiation

Given $(R_l)_{l=1}^N$ one can form tensor $\tilde{\mathcal{T}}$ that approximates tensor $\mathcal{T}$ in the sense of their euclidean distance $||\tilde{\mathcal{T}} - \mathcal{T}||$. This approximation can be exploited to form lossy compression algorithms of signals that are indexed by more than two indices. It should by noted that the choice of $(R_l)_{l=1}^N$ in a given application is non-obvious and depends on the properties of processed signals.

Animated 3D mesh compression using HO-SVD

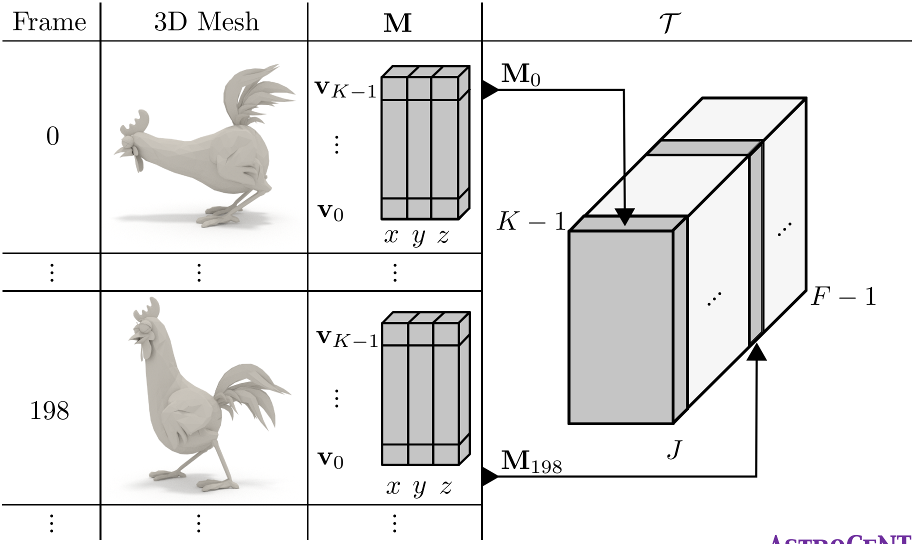

Animated 3D mesh compression — algorithm

Input: Data Tensor $\mathcal{T}$, Compression rate CR, Quality metric d
Output: Quality of $\mathcal{T}'$
`/*` $\mathcal{X}$ `is a normalised tensor */`
`/*` $\mathfrak{R}$ `is a sequence of homography matrices */`
$\mathcal{X}, \mathfrak{R} = \text{Rigid Motion Estimation}(\mathcal{T})$;
`/*` $[\![\mathcal{C}; \mathbf{U}^{(1)}, \mathbf{U}^{(2)}, \mathbf{U}^{(3)}]\!]$ `is the Tucker operator */`
$[\![\mathcal{C}; \mathbf{U}^{(1)}, \mathbf{U}^{(2)}, \mathbf{U}^{(3)}]\!] = \text{HOSVD Decomposition}(\mathcal{X})$;
$[\![\tilde{\mathcal{C}}; \tilde{\mathbf{U}}^{(1)}, \tilde{\mathbf{U}}^{(2)}, \tilde{\mathbf{U}}^{(3)}]\!] = \text{Truncate}([\![\mathcal{C}; \mathbf{U}^{(1)}, \mathbf{U}^{(2)}, \mathbf{U}^{(3)}]\!], R_1, R_3)$
$\tilde{\mathcal{T}} = \text{Reconstruct}([\![\tilde{\mathcal{C}}; \tilde{\mathbf{U}}^{(1)}, \tilde{\mathbf{U}}^{(2)}, \tilde{\mathbf{U}}^{(3)}]\!], \mathfrak{R})$;
return $\tilde{\mathcal{T}}$;

Algorithm 2: Compression and decompression procedure.

ASTROCENT

Animated 3D mesh compression — impact

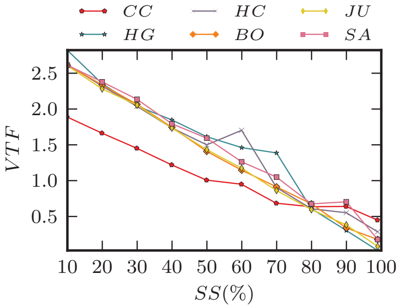

[b]

Figure 4. n impact of HO-SVD parameter selection on MSE reconstruction for the *Chicken* animation. Panel (a) presents the reconstruction error as a function of the number of mode-1 (v) and mode-3 (f) components. Note that the distortion drops sharply with only a few first components. Panel (b) presents Vertices-to-Frame ratio as a function of *SS*

AstroCeNT

Animated 3D mesh compression — chicken detail

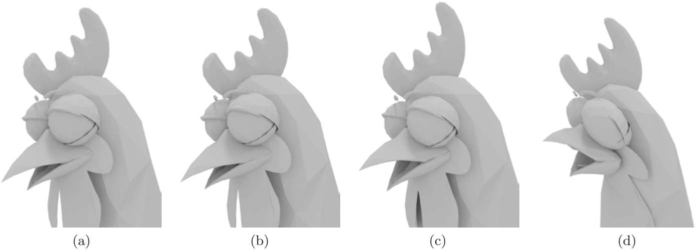

Figure 1. fragment of a reconstructed animation sequence for *Chicken* animation. Panel (a) presents an original model, in further panels the data tensor is compressed to (b): 5.1%, (c): 2.1%, and (d): 1.1% of its original size.

ASTROCENT

Animated 3D mesh compression — chicken

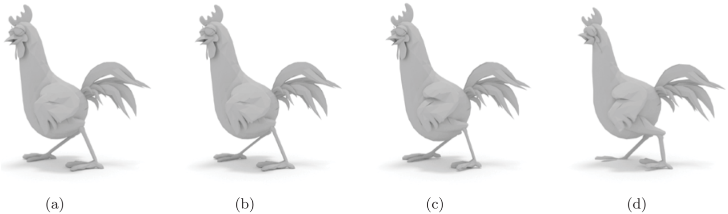

Figure 5. Visualization of a reconstructed model for *Chicken*. (a): original, (b): SS=94.8%, (c): SS=97.8%, (d): SS=98.8%.

ASTROCENT

Animated 3D mesh compression — cow

Figure 6. Visualization of a reconstructed model for *Collapse*. (a): original, (b): SS=69.9%, (c): SS=84.9%, (d): SS=97.9%.

ASTROCENT

Animated 3D mesh compression — dance

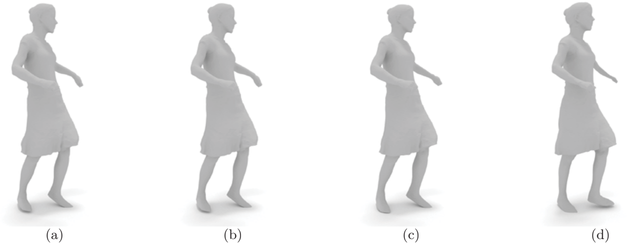

Figure 7. Visualization of a reconstructed model for *Samba*. (a): original, (b): SS=89.9%, (c): SS=94.9%, (b): SS=97.9%.

AstroCeNT

Original

Compressed 90%

Original

Compressed 99%

References

Lieven De Lathauwer, Bart De Moor, and Joos Vandewalle.
A multilinear singular value decomposition.
SIAM journal on Matrix Analysis and Applications, 21(4):1253–1278, 2000.

T. G. Kolda and B. W. Bader.
Tensor Decompositions and Applications.
SIAM Review, 51(3):455–500, September 2009.

Jun-Li Li and Cong-Feng Qiao.
Classification of arbitrary multipartite entangled states under local unitary equivalence.
Journal of Physics A: Mathematical and Theoretical, 46(7):075301, 2013.

Michal Romaszewski, Piotr Gawron, and Sebastian Opozda.
Dimensionality reduction of dynamic mesh animations using ho-svd.
Journal of Artificial Intelligence and Soft Computing Research, 3, 2013.

2-nd edition of comic book on quantum computing

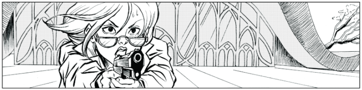

ŚWIAT, JAKI ZNAMY – ŚWIAT WOLNYCH SIECI INFORMACYJNYCH, ŚWIAT SWOBODNEJ WYMIANY WIEDZY I DOŚWIADCZEŃ – SKOŃCZYŁ SIĘ NIEODWOŁALNIE. WOLNY DOSTĘP DO WIEDZY OKAZAŁ SIĘ SZKODLIWĄ IDEĄ, A NAJBARDZIEJ SKORZYSTALI NA NIM ZBRODNIARZE, TWÓRCY BRONI BIOLOGICZNEJ, KTÓRA NIEOMAL ZMIOTŁA CYWILIZACJĘ Z POWIE-RZCHNI ZIEMI. ZDZIESIĄTKOWANA PRZEZ TERROR, WOJNY I EPIDEMIĘ LUDZKOŚĆ POWOLI ODRADZA SIĘ POD CZUJNYM OKIEM CERBERA. JEGO AGENCI MAJĄ JEDEN CEL: NIE DOPUŚCIĆ, ABY WIEDZA STAŁA SIĘ ZNÓW POWSZECHNIE DOSTĘPNA.

JEDNAK WSZECHOBECNA CENZURA RODZI BUNT.

NIEKTÓRZY SĄ NAWET GOTOWI GINĄĆ – I ZABIJAĆ – ZA WOLNY DOSTĘP DO INFORMACJI. I NAJWYRAŹNIEJ CZUJĄ SIĘ DOŚĆ PEWNIE, BY RZUCIĆ CERBEROWI WYZWANIE – BO CZYM INNYM MOŻE BYĆ ZAMACH NA WYSOKIEGO DYGNITARZA ORGANIZACJI W JEJ GŁÓWNEJ KWATERZE? TERAZ CERBER MUSI UŻYĆ WSZYSTKICH DOSTĘPNYCH ŚRODKÓW, BY ZNALEŹĆ ZLECENIODAWCÓW NAPASTNIKA. NIESTETY, JEGO AS ATUTOWY, KWANTOWA HAKERKA EVE, WŁAŚNIE ZASIADA NA ŁAWIE OSKARŻONYCH POD ZARZUTEM ZDRADY NA RZECZ GRUPY TERRORYSTYCZNEJ ALICE...

Wydanie przygotowane przy wsparciu

BNP PARIBAS

IBM

QZ quantumz.io

IITiS PAN Instytut Informatyki Teoretycznej i Stosowanej

AstroCeNT

O komputerach kwantowych, przewadze kwantowej czy kryptografii kwantowej pisze się już nie tylko w artykułach naukowych. Dzisiaj niemal co krok można natrafić na wiadomości o kolejnych praktycznych zastosowaniach aplikacji algorytmów kwantowych, np. w obszarze finansów czy chemii molekularnej. Chcieliśmy przybliżyć Ci zagadnienia związane z informatyką kwantową (a szczególnie z komunikacją kwantową) w sposób na tyle intuicyjny, na ile jest to możliwe bez rezygnowania z rygoru matematycznego.

Dlatego oddajemy w Twoje ręce nietypową publikację, składającą się z dwóch części: pierwsza to komiks akcji, którego tematyka nawiązuje do pewnych zagadnień informatyki kwantowej, druga – merytoryczna – to podręcznik z wyłożonymi podstawami tej dziedziny. Obie te części możesz czytać niezależnie od siebie. W części merytorycznej wymagamy od Ciebie umiejętności dokonywania operacji na liczbach rzeczywistych, rozumienia pojęcia układu współrzędnych, znajomości podstaw trygonometrii i elementarnych pojęć rachunku prawdopodobieństwa. W książce znajduje się jednak rozdział z repetytorium matematycznym, w którym odnajdziesz wszystkie niezbędne informacje, aby wykonywać podstawowe obliczenia informatyki kwantowej.

Masz zatem przed sobą książkę-eksperyment; jako jej autorzy liczymy, że będziesz się przy niej dobrze bawić – niezależnie od tego, czy przeczytasz jedną, czy obie jej części.

Książka została przygotowana przy współpracy z BNP Paribas Bank Polska S.A., IBM Polska Sp. z o.o. oraz Zakładem AstroCeNT Centrum Astronomicznego im. Mikołaja Kopernika Polskiej Akademii Nauk.

ISBN 978-83-962049-0-5

9 788396 204905

Thank you

ASTROCENT

ASTROCENT
European Funds Smart Growth
Republic of Poland
FNP Foundation for Polish Science
European Union European Regional Development Fund
CAMK PAN